An efficient, compact and low-cost Dual Cylinder Hydrostatic Actuator (DCHA)

Travis Wiens

Taylor & Francis
Taylor & Francis Group

An efficient, compact and low-cost Dual Cylinder Hydrostatic Actuator (DCHA)

Travis Wiens

Department of Mechanical Engineering, University of Saskatchewan, Saskatoon, Canada

ABSTRACT

Pump-controlled systems are highly efficient alternatives to the high throttling losses of valve-controlled systems. Closed-circuit systems have been widely adopted for rotary loads, but the asymmetrical nature of linear actuators has limited their acceptance. Hydrostatic linear actuators typically are costly or complex, inefficient or exhibit low force density. This paper presents a Dual Cylinder Hydrostatic Actuator, which is highly efficient for both resistive and overrunning loads, uses commercially available low-cost components, and provides the same high force of a conventional system in a similarly sized system. A steady-state model is presented, along with an experimental validation on a small-scale apparatus. An analysis of a full-scale application is performed, including strategies for mitigation of energy losses.

Introduction

Closed-circuit or hydrostatic hydraulic systems are widely applied in industry for rotary loads, particularly ground drive transmissions (Merritt 1967, Costa and Sepehri 2015). They have high power and torque density, good controllability and have the ability to recover energy to the shaft during braking or other overrunning conditions. However, application of closed-circuit systems to linear actuators has lagged, primarily due to the asymmetrical nature of single-rod cylinders.

Hydrostatic transmissions rely on the fact that the flow returning from the load is substantially the same as the pump output. The return flow can then be applied to the pump inlet, allowing for four-quadrant load control via pump displacement without the need for throttling valves. However, typical single-rod hydraulic cylinders have a differential piston area so the rod-end flow will be less than the head-end flow, making them unsuitable for closed-circuit operation.

A number of schemes to work around this have been applied, but without widespread industrial adoption. One of the most common is the double-rod cylinder (Merritt 1967, Grabbel and Ivantysynova 2005, Lei *et al.* 2011, McCullough 2011). With a secondary rod to balance the piston areas, this system can be easily used for hydrostatic systems. However, there are a number of drawbacks: the second rod does not perform useful work but takes up space at the rear of the cylinder while reducing the effective piston area, thereby considerably reducing the force density of the actuator.

Others have developed single-rod symmetrical cylinders. These cylinders typically have complex internal geometries that are costly to produce, including multiple chambers and sealing surfaces (e.g. Habibi and Goldenberg 1999, Hindman 2006). They also achieve symmetrical areas by reducing the head-end piston area, necessarily reducing the maximum force. Combined with the increased mass of their internal structure, they exhibit lower mass and volume force densities than conventional systems.

Rotary devices can be used to balance the flow, known as synchronisers or hydraulic transformers (Achten and Palmberg 1999, Fales and Raab 2005; etc.). These systems are efficient, but the flow-balancing unit reduces the available force, increases cost, mass and complexity, and reduces force density.

Yet another strategy is to the simply ignore the flow imbalance and allow the excess to be vented via relief valves or sourced via check valves (or using pilot-operated check valves or shuttle valves), reducing the fraction of available energy recovered (Rahmfield and Ivantysynova 2001, Jalayeri *et al.* 2015). These systems require either an accumulator or relatively large charge pump to source the unbalanced flow when extending the cylinder. A system mounted on an excavator found this type of system to be considerably more efficient than a valve-controlled system, but the energy recovery was negligible (Williamson *et al.* 2008). Another challenge with this type of system is instability; Williamson and Ivantysynova (2008) noted an instability caused by an interaction between the pilot-operated check valves and load at low velocity. In 2010, the
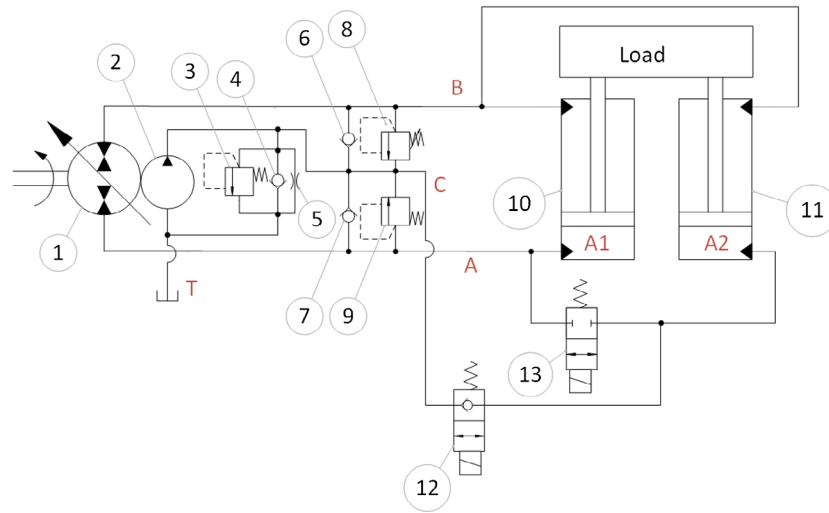
CONTACT Travis Wiens ✉ t.wiens@usask.ca

Figure 1. System schematic, showing main pump, 1; charge pump, 2; charge pump relief, 3 and anticavitation check, 4; cooling flow orifice, 5; workport anitcavitation valves, 6 & 7; workport relief valves, 8 & 9; cylinders, 10 & 11; HE mode valve, 12; and HF mode valve, 13.

Table 1. Selected steady-state model parameters.

	Small-Scale Apparatus	Full-Scale Simulation	Note
	0.61	0.61	1
ρ (kg/m³)	890	890	2
v (cSt)	68	68	2
ω (rev/min)	1750	2200	3
D_{max}(cc/rev)	21.8	40.6	2
D_C(cc/rev)	4.1	6.9	2
A_A(mm²)	804	3117	2
A_B(mm²)	424	1527	2
F_c (N)	452	1752	3
B_f (N/(m/s))	2254	8740	3
A_{CT} (mm²)	1.812	0	3,4
R_{AB} (Pa/(m³/s))	5.07x10¹¹	3.01x10¹¹	3
R_{AT}, R_{BT} (Pa/(m³/s))	3.11x10¹²	1.85x10¹²	3
A_{CA2} (mm²)	242	242	2
A_{A1A2} (mm²)	33.9	242	2
A_{RVCmax} (mm²)	4.32	100	3
A_{CVCmax} (mm²)	20	100	1
A_{RVAmax} (mm²)	10	100	1
A_{CVAmax}, A_{CVBmax} (mm²)	30.2	100	3
K_{RVB} (m²/Pa^{1/2})	2.61×10^{-9}	7.83×10^{-8}	3

Notes: 1. Estimated value.
2. Value from product literature.
3. Small-scale apparatus value determined experimentally,.
4. Large-scale apparatus has no cooling orifice.

same authors proposed a pressure feedback controller to stabilise the system (Williamson and Ivantysynova 2010). Others have proposed different stabilising control schemes, including Wang *et al*. 2011 who introduced controlled leakage to stabilise the system, and Çalışkan *et al*. (2015) who proposed an underlapped shuttle valve.

For a more in-depth review of recent literature, please refer to Costa and Sepehri (2015).

Proposed system

As first proposed in preliminary form in Wiens and Bitner (2016), the Dual Cylinder Hydrostatic Actuator (DCHA) is shown in Figure 1. This system uses two conventional single-rod cylinders (items 10 and 11),

each with a 2:1 piston area ratio. In High Efficiency (HE) mode, the A port of the closed-circuit pump is connected only to the head end of one cylinder (item 10) and the B port is connected to both rod-end chambers. The other head-end chamber (item 11) is connected to low pressure via the energised solenoid valve 12 (in this case supplied by a charge circuit). The single head-end flow is approximately equal to the two rod-end flows, so the flows are balanced.

Like other closed-circuit systems with symmetric actuators, this mode exhibits half the maximum extending force of an open-circuit system with similarly sized single-rod cylinders, but double the maximum extending velocity and the ability to recover energy to the shaft when braking or lowering a load. The system presented here does not store recovered energy, but it is transferred to the shaft where is can be applied to other loads, parasitic engine losses, or stored in flywheel or other energy storage device.

When high forces are required, solenoid valve 13 is energised and valve 12 is deenergised, connecting the second head-end chamber (item 11) to the pump. This High Force (HF) mode allows the system to provide the full force and velocity of a similarly sized open circuit system with a single-rod cylinder, that is, double the extending force of HE mode and half the extending velocity. This mode has some losses over the relief or check valves required to balance the flow, but there is no throttling of the main flow, so it is still relatively efficient. This mode has the ability to recover energy, but at a reduced effectiveness. Note that this system does not use shuttle or pilot-operated check valves (as used in Rahmfield and Ivantysynova 2001), so does not suffer from instability problems noted above, at the cost of a small efficiency decrease.

As will be seen in later sections, this system is highly efficient over a wide range of operating conditions. It is
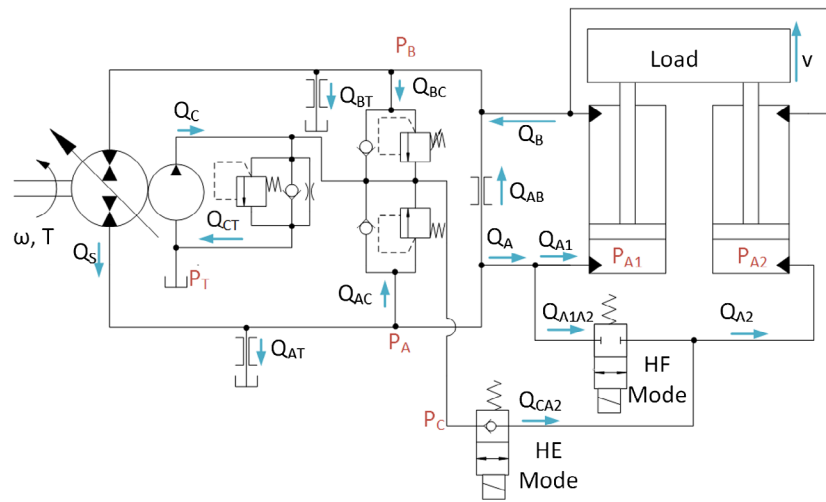
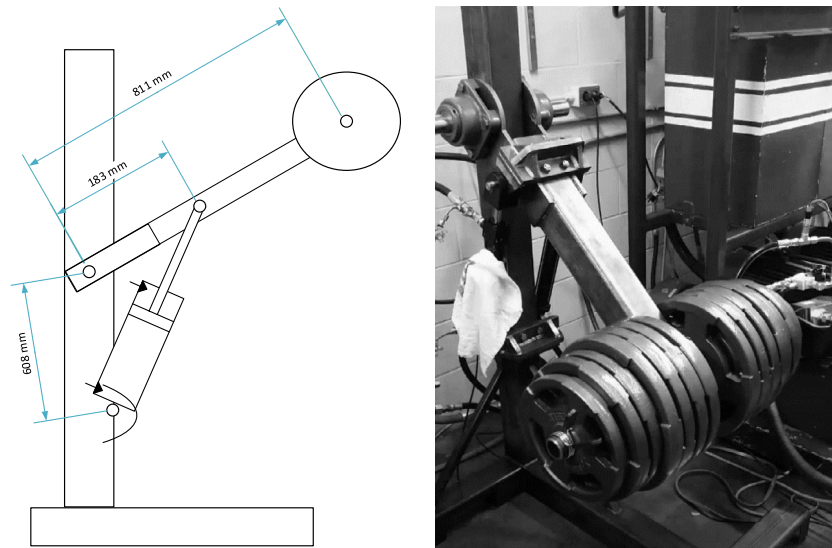**Figure 2.** System schematic as modelled, showing nomenclature and virtual resistances.

Figure 3. Experimental apparatus.

Table 2. Experimental instrumentation.

Quantity	Instrumentation	Range	Output type
Cylinder Position	MTI Instruments model LTC-300–200-SA laser displacement transducer	0–300 mm	0–5 V
Swash Plate Angle	Lucas RVDT model 02560234–000	+/−30°	+/−0.375
Charge Pump Pressure	STW model M01-CAN	0–7 MPa	J1939
Other Pressures	STW model M01-CAN	0–25 MPa	J1939
Temperature	Omega HH92 Thermocouple reader	−40–300 °C	Display

also comparable in mass or volumetric force density to a valve-controlled system: the main pump is of comparable size to a load-sensing pump, and the two solenoid valves and a charge pump would be expected to have similar combined size as the eliminated throttling valves.

This system uses all conventional, commercially available components, including cylinders, pumps and valves, having an overall complexity and cost comparable to that of a conventional load-sensing system, especially if the conventional system already uses dual cylinders, as is commonly seen on machinery such as excavators and wheel loaders.

Steady-state model

A steady-state model was developed in order to examine hydraulic energy efficiency and study the relative magnitudes of energy losses in the system. The major assumption in this model is steady-state operation: due to the finite cylinder stroke, the system does not truly reach steady state before reaching the end of stroke. However, the approximately linear response of small fluctuations around an operating point means that the average performance of the oscillating system will be similar to the steady-state characteristics.
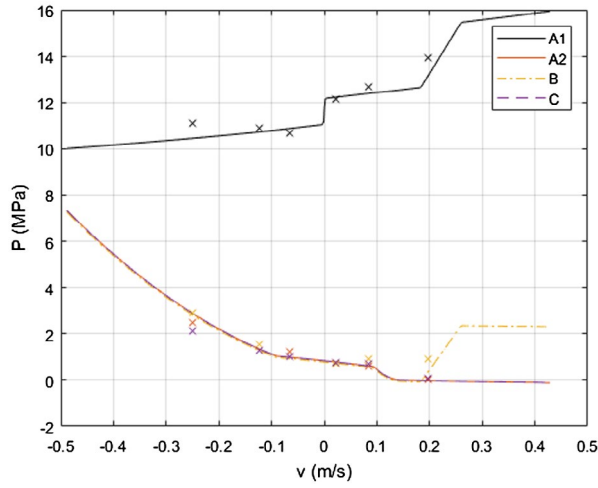
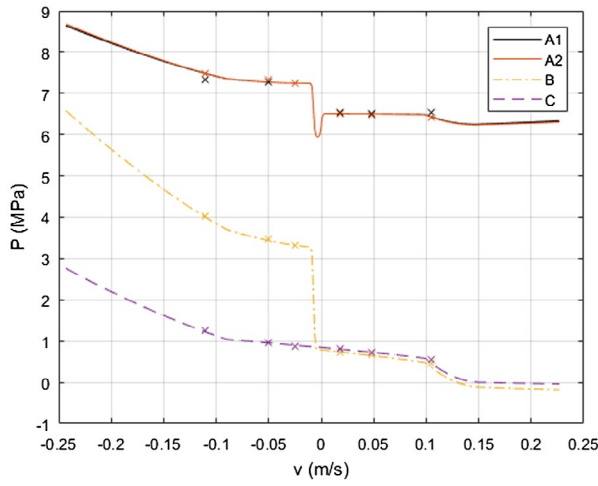**Figure 4.** Experimental and modelled pressures for HE mode, with a 9.3 kN load.

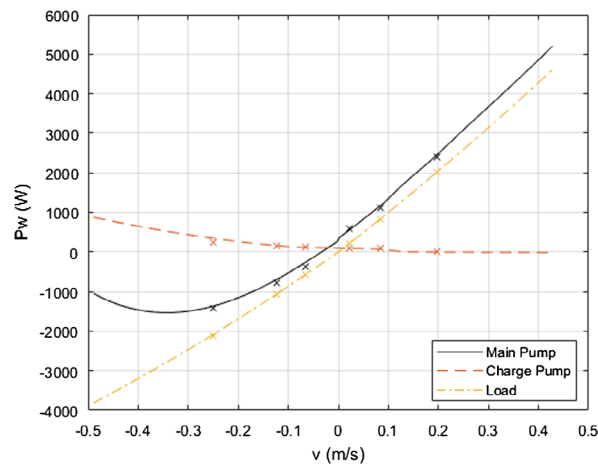**Figure 5.** Experimental and modelled pressures for HF mode, with a 9.3 kN load.

Figure 6. Experimental and modelled hydraulic power for HE mode, with a 9.3 kN load. Negative pump powers denote energy recovery.
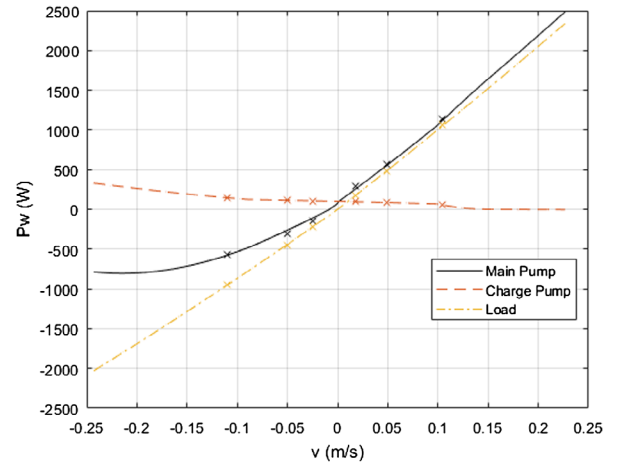

Figure 7. Experimental and modelled hydraulic power for HF mode, with a 9.3 kN load.

Figure 2 shows pressure and flow nomenclature for the model. The main pump is assumed to be an ideal variable displacement pump with perfect displacement control. Thus the pump flow, Q_s, is given by

$$Q_s = \frac{\omega D}{2\pi} \tag{1}$$

where ω is the shaft angular speed (rad/s) and D is the pump's displacement (m³/rev). The pump's internal and external leakage, Q_{AB}, Q_{AT} and Q_{BT}, are assumed to be laminar:

$$Q_{AB} = \frac{P_A - P_B}{R_{AB}} \tag{2}$$

$$Q_{AT} = \frac{P_A - P_T}{R_{AT}} \tag{3}$$

$$Q_{BT} = \frac{P_B - P_T}{R_{BT}} \tag{4}$$

where R_{AB}, R_{AT} and R_{BT} are the effective resistances of each leakage path and pressures are as labelled in Figure 2.

The charge pump is assumed to be an ideal fixed displacement pump, with flow given by

$$Q_C = \frac{\omega D_C}{2\pi} \tag{5}$$

where D_C is the pump displacement.

Flows between the charge pump outlet and tank are modelled as a relief valve, anti-cavitation valve and orifice in parallel (this 'cooling orifice' regulates cooling flow to the rotating group). In order to avoid numerical issues for flows near zero, each orifice is modelled
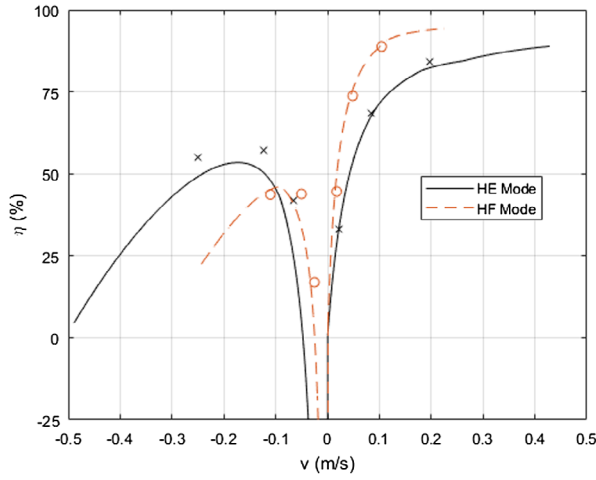
Figure 8. Experimental and modelled hydraulic efficiency for HE and HF mode, with a 9.3 kN load.
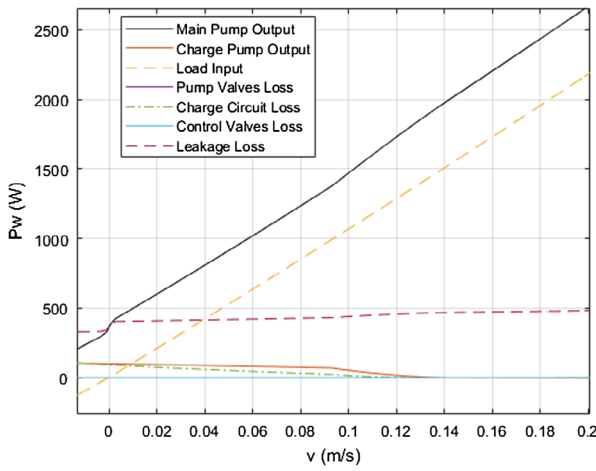

Figure 9. Modelled pump and load power as well as losses for a 10 kN external load in HE mode.

Figure 10. Enlarged view of Figure 9 for small lifting velocities.
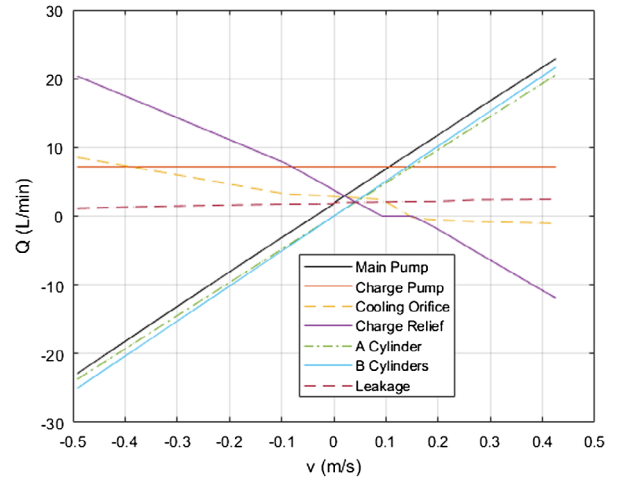
Figure 11. Selected flows, in HE mode for a 10 kN external load.

as a two-stage laminar-turbulent orifice following the method of Ellman and Piche (1999), requiring parameters of discharge coefficient C_d, fluid density ρ, fluid viscosity ν and critical Reynolds number Re_{cr}. The relief valve and check valve orifice areas linearly increase from zero at the cracking pressure to a maximum area over the pressure override range. Therefore, the combined flow, Q_{CT}, is given by

$$Q_{CT} = Q_{or}\left(A_{\mathrm{RVCT}}, P_C - P_T\right) - Q_{or}\left(A_{\mathrm{CVCT}}, P_T - P_C\right) \\ + Q_{or}\left(A_{CT}, P_C - P_T\right) \quad (6)$$

where $Q_{or}(A, \Delta P)$ is Elmann's two-stage orifice function, A_{CT} is the cooling orifice area. The relief and check valve areas, denoted by subscripts RV and CV above, are each given by

$$A(\Delta P) = \begin{cases} 0 & \text{if } \Delta P \leq P_{cr} \\ A_{\max} & \text{if } \Delta P \geq P_{cr} + P_{or} \\ \frac{\Delta P - P_{cr}}{P_{or}} A_{\max} & \text{otherwise} \end{cases} \quad (7)$$
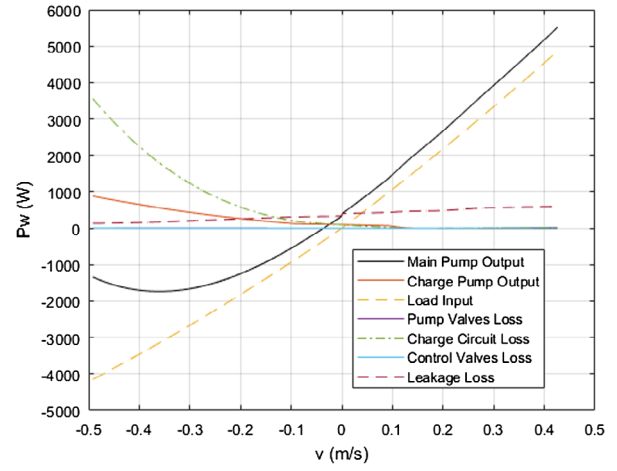
where P_{cr} is the cracking pressure, P_{or} is the pressure override range and $A_{\max}$ is the maximum orifice area for each valve.

The pump's workport A relief and anticavitation check valves are modelled as above, again with linear orifice area:

$$Q_{AC} = Q_{or}\left(A_{\mathrm{RVAC}}, P_A - P_C\right) - Q_{or}\left(A_{\mathrm{CVAC}}, P_C - P_A\right) \quad (8)$$

where these valves' orifice areas, A_{RVAC} and A_{CVAC}, are defined as in Eq. (7).

In order to allow for adjustment of setpoint pressure, an external relief valve was installed on workport B, which had a different opening characteristic. In this case

$$Q_{BC} = Q_{or}\left(A_{\mathrm{RVBC}}, P_B - P_C\right) - Q_{or}\left(A_{\mathrm{CVBC}}, P_B - P_C\right) \quad (9)$$

$$A_{\mathrm{RVBC}}(\Delta P) = \begin{cases} 0 & \text{if } \Delta P \leq P_{cr} \\ K_{\mathrm{RVB}}\sqrt{\Delta P - P_{CR}}\tanh\left(\frac{\Delta P - P_{CR}}{P_{\mathrm{ref}}}\right) & \text{otherwise} \end{cases} \quad (10)$$
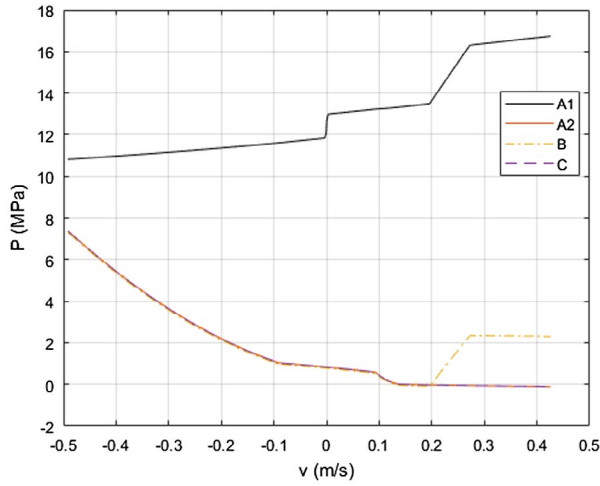
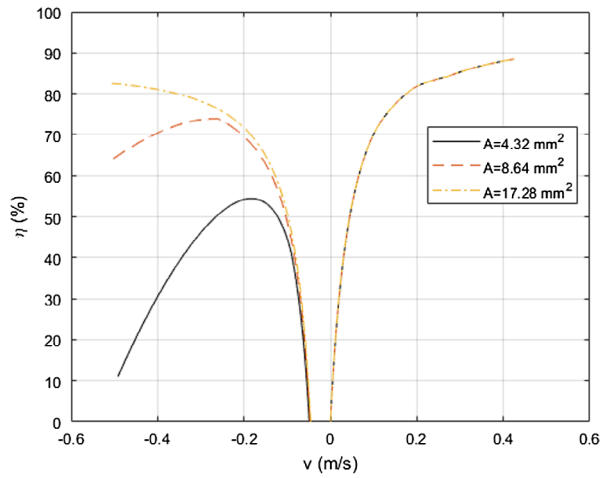**Figure 12.** Pressures in HE mode for a 10 kN external load.

Figure 13. Effect of increasing charge circuit relief valve maximum orifice area on HE mode hydraulic efficiency.

where K_{RVB} is an area-related constant, and a tanh function is used to smooth the infinite derivative near zero area, with the extent of the distortion controlled by P_{ref}. The check valve area, A_{CVBC} follows the linear area relationship in Eq. (7).

The cylinder is modelled as an ideal cylinder with no leakage (experimentally, cylinder leakage is lumped with the pump's R_{AB} in Eq. (2) although it is small relative to pump leakage). The flow into and out of each cylinder's head end is

$$Q_{A1} = Q_{A2} = A_A v \qquad (11)$$

where A_A is the piston head area and v is the cylinder's extending velocity. The combined flow from both rod end chambers is

$$Q_B = 2A_B v \qquad (12)$$

where A_B is the rod end piston area of a single cylinder.

The forces acting on the cylinders are assumed to include an external force F, and viscous and Coulomb friction, given by

$$F_f = F_c \tanh\left(\frac{v}{v_{ref}}\right) + B_f v \qquad (13)$$

where F_c is the ideal Coulomb friction force, B_f is the viscous damping coefficient and tanh is used instead of a sign function to avoid discontinuities around zero velocity. The velocity v_{ref} is used to control what is considered a 'small' velocity around zero. The net force on the cylinders is then

$$F_{net} = P_{A1}A_A + P_{A2}A_A - P_B 2A_B - F - F_f \qquad (14)$$

For numerical convenience, the solenoid valves are assumed to be ideal orifices with fully turbulent flow (i.e. no laminar region), only one of which may be open at a time. Therefore, in High Efficiency mode

$$P_{A2} = P_C - \frac{\rho}{2}\frac{Q_{CA2}|Q_{CA2}|}{(C_d A_{CA2})^2} \qquad (15)$$

$$Q_{A1A2} = 0 \qquad (16)$$

$$Q_{CA2} = Q_{A2} \qquad (17)$$

where A_{CA2} is the HE valve's orifice area. Alternately, while in High Force mode:

$$P_{A2} = P_A - \frac{\rho}{2}\frac{Q_{A1A2}|Q_{A1A2}|}{(C_d A_{A1A2})^2} \qquad (18)$$

$$Q_{A1A2} = Q_{A2} \qquad (19)$$

$$Q_{CA2} = 0 \qquad (20)$$

where A_{A1A2} is the HF valve's orifice area.

Assuming constant density, flow continuity equations give net flows at points B, A1 and C as

$$Q_{Bnet} = Q_B - Q_S - Q_{BC} + Q_{AB} - Q_{BT} \qquad (21)$$

$$Q_{A1net} = -Q_{A1} - Q_{AB} - Q_{A1C} + Q_S - Q_{A1A2} - Q_{AT} \qquad (22)$$

$$Q_{Cnet} = Q_C + Q_{BC} + Q_{A1C} - Q_{CT} - Q_{CA2} \qquad (23)$$

The above equations constitute a non-linear system of equations that must be solved to determine the steady-state operating point. This was achieved using the Matlab 'fsolve' function to numerically solve for values of P_A, P_B, P_C and v that set the left-hand side of Equations (14), (21), (22), and (23) to zero.

The major performance metric used here is the hydraulic efficiency, defined in Weng (1966), Jarboe (1983), van der Burgt (1994) and Vukovic et al. (2017) as the ratio of useful hydraulic power to available hydraulic power. In this case, if the load is consuming power, this is the ratio of load power to total pump output power, and the inverse in the overrunning case:
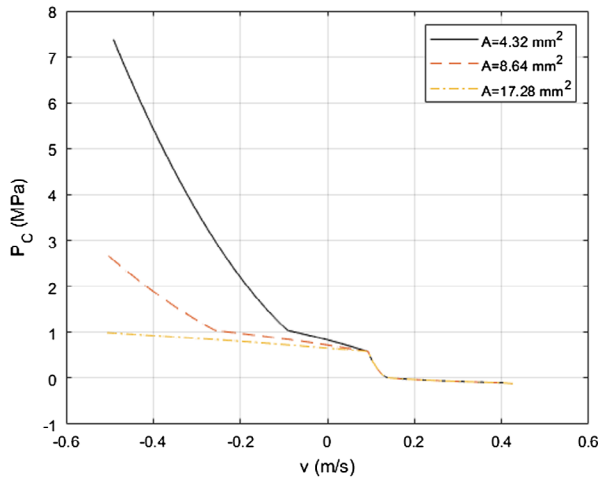
Figure 14. Effect of increasing charge circuit relief valve maximum orifice area on HE mode charge circuit pressure.
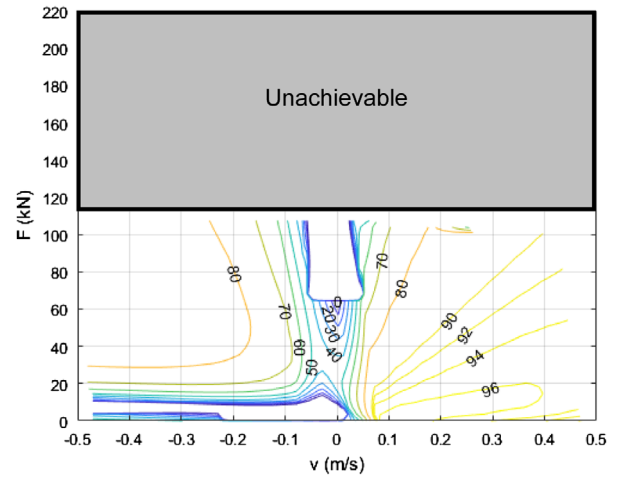

Figure 15. Hydraulic efficiency map for full-scale system in High Efficiency mode.
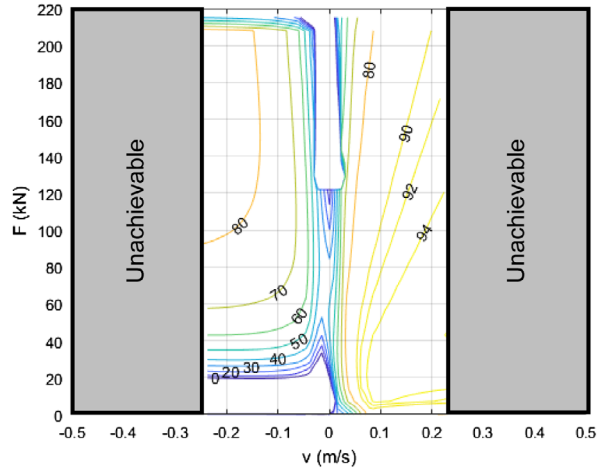

Figure 16. Hydraulic efficiency map for full-scale system in High Force mode.

Figure 17. Hydraulic efficiency map for a comparable load-sensing system. The efficiency for negative velocities is less than zero as no energy recovery is possible.

$$\eta = \begin{cases} \dfrac{Pw_L}{Pw_S + Pw_C} & Pw_L \geq 0 \\ \dfrac{Pw_S + Pw_C}{Pw_L} & Pw_L < 0 \end{cases} \qquad (24)$$

where the load, main pump and charge pump powers are

$$Pw_L = Q_{A1}P_{A1} + Q_{A2}P_{A2} - Q_B P_B \qquad (25)$$

$$Pw_S = Q_S P_A - Q_S P_B \qquad (26)$$

$$Pw_S = Q_C P_C - Q_C P_T. \qquad (27)$$

One deficiency in the above efficiency definition occurs when the load is overrunning ($Pw_L < 0$) but also the pumps are supplying net hydraulic power, i.e. $(Pw_S + Pw_C) > 0$. This situation, where there both the load and pump are supplying energy to the hydraulic system, results in an negative efficiency with little physical meaning, which goes to negative infinity as the load power approaches zero. Thus, a negative efficiency should be viewed as bad (as we are powering the pump when we should be recovering energy), but the magnitude is not useful for comparison.
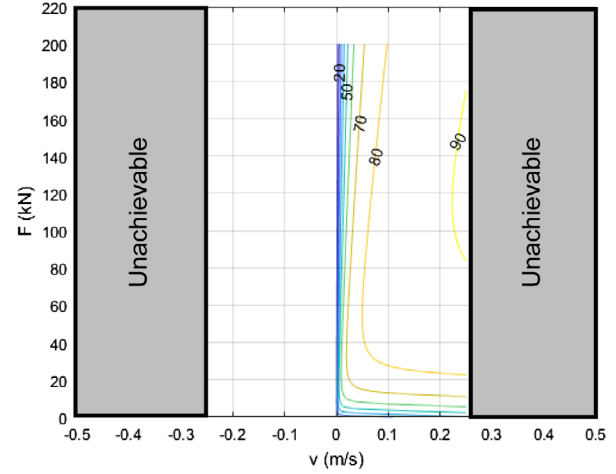
Small-scale experimental apparatus

An experimental apparatus was built to validate the above system of equations. This was constructed using a Hydo-Gear model PY pump. This is a hydrostatic pump designed for use on lawn equipment, with a main pump maximum displacement of 21.8 cc/rev and a 4.1 cc/rev charge pump. The pump integrates workport check and relief valves as well as charge pump relief valve with experimentally determined parameters found in Table 1. It also includes an integrated nozzle to provide cooling flow to the rotating group (item 5 in Figure 1). An additional check valve (item 4 in Figure 1.) was included to avoid cavitation at the charge pump outlet. The pump was run by a 20 HP electric motor at 1750 rpm. This motor is oversized for this application, to ensure a constant shaft speed.

In order to allow for adjustment of the workport B relief pressure, an external relief valve was installed (item 8 in Figure 1), Hydraforce model RV08-22, set with a
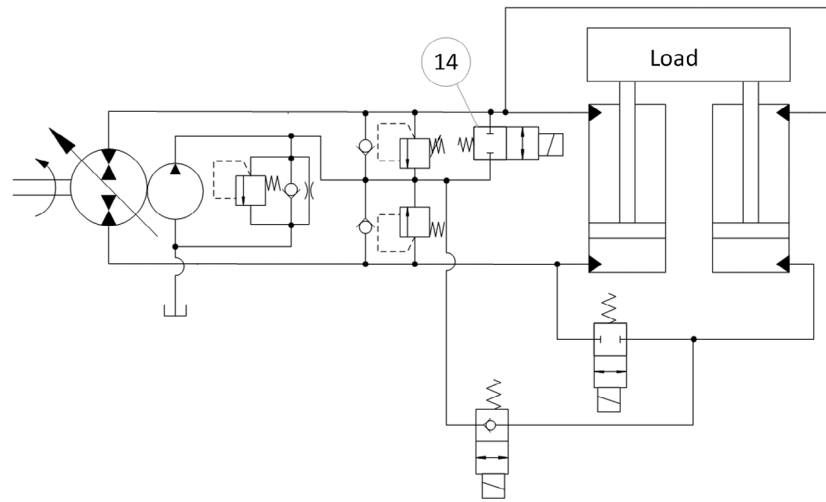
Figure 18. Addition of a solenoid valve, item 14. This valve reduces relief valve losses in HF mode, without the stability problems of a pilot-operated check valve.

cracking pressure of 3.5 MPa. The experimentally determined parameters are found in Table 1. The solenoid valves used to control the modes were Parker model DSL102C for the HF valve and a Hydraforce SF20-22 for the HE valve. Note that the HE valve must be larger than the HF valve to avoid the possibility of cavitation, but the selected valve is still oversized.

Solenoid valves were controlled over a J1939 bus via Hydraforce EVDR 201A valve drivers. The pump's swash plate position was controlled using a rotary hydraulic actuator with a separate power supply, operated by a servo valve controlled with an analogue proportional closed loop controller.

A load was provided by the apparatus shown in Figure 3. This allows for a gravitational and inertial loading, using up to 247 kg of weight, which can apply up to 13.8 kN of force to the cylinders. This apparatus was designed to mimic the non-linear force characteristics of a front-end loader, in smaller scale.

Experimental instrumentation is listed in Table 2. J1939 signals were acquired using a Vector CANboard XL interface, while analogue signals were acquired using a National Instruments PCIe-6251 interface. All data were logged at a 10 ms sample rate.

Experimental model validation

Figures 4 and 5 show the effect of cylinder velocity on pressures in HE and HF mode, with both model and experimental values. These data were recorded with the apparatus loaded with 204 kg of weights, which corresponds to approximately 9.3 kN force at the cylinders when the boom is horizontal. Note the different y-axis scales, reflecting the higher pressures required in HE mode.

Figures 6 and 7 show the main pump, charge pump and load hydraulic power (i.e. pressure times flow in each case). The load flows are calculated from load velocity and the pump nominal flow is calculated from swash plate angle. Therefore, the hydraulic system efficiency calculated from this data (shown in Figure 8), includes the effect of leakage (volumetric efficiency), but not mechanical frictional losses in the pump or load (mechanical efficiency) or servo losses required to position the swash plate. It should be noted that servo losses can be a significant portion of losses in an efficient system (Rahmfield and Ivantysynova 2001), but they will also exist in most comparable valve-controlled system, and the relatively stable swash plate position in a displacement-controlled architecture can be expected to require less pump controller flow than a pressure-controlled pump (Lux and Murrenhoff 2016). Thus, comparative numbers are fair, if not advantageous to conventional load sensing systems. Additionally, in the ideal case, servo losses only occur when the pump displacement changes, which does not occur in the steady-state analysis presented here.

These data show good agreement between model and experiment. One area where the model and experiment do show some disagreement was for the 0.2 m/s velocity point in HE mode. In this situation, the model predicts the requirement of flow through the charge pump check valve (item 4 in Figure 1) to prevent cavitation. We did not measure any pressures below atmospheric during this test and did not detect any signs of cavitation when the check valve was blocked. The discrepancy may be due to unmodelled leakage in the system, overestimated pressure losses or an unmodelled increase in charge pump volumetric efficiency under these situations. In any case, while cavitation is important from a practical standpoint, the flows and the pressure differences are small and will likely result in a small change in the resulting efficiency analysis.
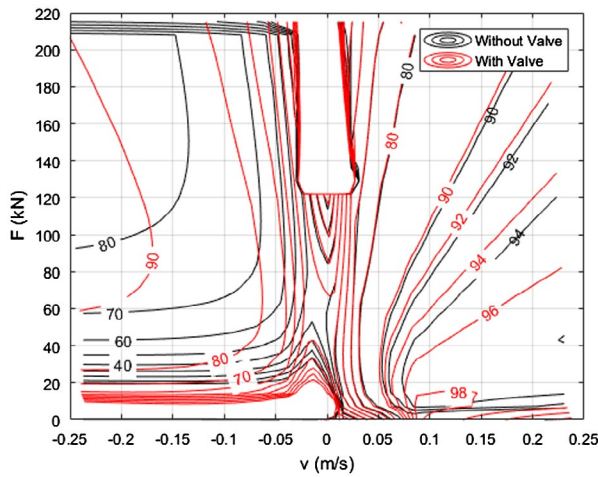
Figure 19. Hydraulic efficiency maps in HF mode with and without Port B bypass solenoid valve, showing small increase in efficiency for positive velocities (extending) but large improvements for negative velocities (retracting).
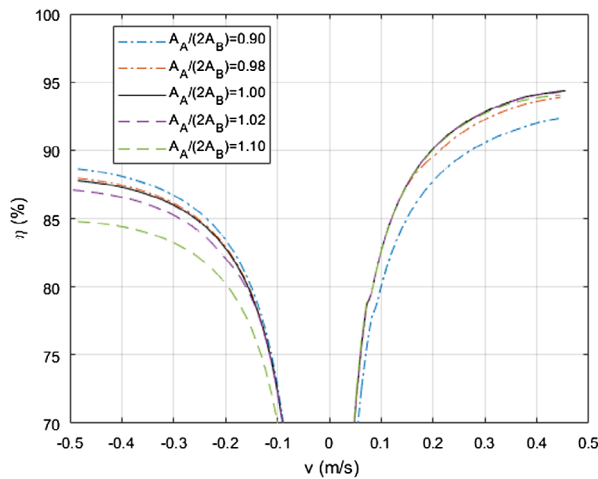

Figure 20. Effect of cylinder area ratio imbalance on hydraulic efficiency, for a force of 50 kN.

Efficiency analysis

The experimental apparatus and results shown above agree with the model, but do not show particularly good performance, especially at low velocities. Notice that the High Force mode shows better hydraulic efficiency than High Efficiency mode when lifting. This is largely due to the mismatch between the pump and load. In the data shown above, the pump is not operated at its maximum flow, so its volumetric efficiency suffers. This is shown in Figures 9 and 10, comparing the modelled power and losses in the system. Note that the leakage losses are approximately constant with load velocity, which dominate the hydraulic efficiency at low flows. Thus, a better efficiency curve can be expected by either selecting a pump with less leakage or using more flow by increasing the cylinder size (also increasing the maximum force).

The left side of Figure 9 also requires comment. When lowering the load, one expects to recover much of the available power. However, in this case, much of

the power is lost to the charge pump circuit, especially at higher speeds. This due to the fact that, when retracting the cylinders in HE mode, the flow from the head end of cylinder 2 exits the system via the charge pump relief valve and cooling orifice. As shown in Figures 11 and 12 for velocities below −0.1 m/s, this saturates the charge pump relief valve and the pressure rises, causing considerable power increase at the charge pump. This use is well outside of the intended use of this charge circuit relief valve, which normally only has to handle the excess charge pump flow. If we enlarge the charge circuit relief valve to handle the flow, the situation is considerably improved. As shown in Figures 13 and 14, if one doubles the valve's orifice area, it still saturates, but the hydraulic efficiency is greatly improved. If we double the area again, the valve no longer saturates and leakage becomes the significant loss.

Full-scale simulation result

The experimental and simulation results presented above are for a small-scale system and were not expected to be optimal. This section will present a full-scale simulation study, intended to represent the boom lift circuit of the front-end loader of a backhoe tractor.

Parameters used for this simulation are found in Table 1. These parameters are based on a John Deere 410G backhoe loader, cylinders dimensions according to ISO 6020-2 and an Eaton model 72400 closed-circuit pump.

Hydraulic efficiency maps for the system in both High Efficiency and High Force modes are shown in Figures 15 and 16, plotted with the same scale for ease of comparison. Note that, for this system, High Force mode is actually more efficient over most of its range of positive velocities (extending), meaning that High Efficiency mode would only be used for recovering energy while retracting and for high velocities that HF mode cannot achieve.

For comparison, the hydraulic efficiency map for an ideal load-sensing system is shown in Figure 17. This assumes a pump with similar displacement and leakage characteristics connected to the same cylinders, with a load sense margin of 1 MPa. It also assumes no additional valve metering losses so the calculated efficiency is somewhat conservative. Both modes of the DCHA are more efficient that the load-sensing system over the entire operating range except for very small extending velocities. Also note that this load-sensing system cannot reach the high velocities achievable by the DCHA in HE Mode.

The efficiency of the system while lowering in High Force mode can be further improved with the addition of an additional solenoid valve, as shown in Figure 18. In HF mode, when the cylinder is retracting, approximately twice as much fluid exits the cylinders as enters, with the excess flow venting to the charge system. Without this

solenoid valve, this occurs when P_B exceeds the work-port relief valve setpoint pressure, causing the energy in a large volume of pressurised fluid to be lost. With the addition of a parallel solenoid valve, this fluid can be vented at low pressure, reducing the energy loss, as shown in Figure 19. As this limits the maximum rod end pressure, the maximum negative force is limited in High Force mode; however, there is no difference in the maximum negative force between HE and HF mode, so HE mode can be used in this situation. An efficiency increase can also be achieved for a similar reason by bypassing the check valve when extending, although the pressure drop is much smaller, so the magnitude of this effect is smaller. This valve provides a similar functionality as the pilot-operated check or shuttle valve seen in other implementations, but does not contribute to instability issues seen with these valves.

Related to this effect is the influence on cylinder area matching. In HE mode, ideally the flow out of the rod-end chambers would equal the flow into a single head-end chamber ($A_A/(2A_B) = 1$). In this case, there is little makeup flow required through either workport check or relief valves. However, realistic cylinders are not perfectly balanced. For example, the ISO 6020-2 metric dimensions used for this simulation specify a 64 mm bore and 45 mm rod diameter. This is the nearest mm to the ideal area ratio, but is not perfect. In this case, $A_A/(2A_B) = 1.02$, meaning approximately 2% of the flow is unbalanced. Similarly, in inch-sized cylinders, the closest ratio for a 2.5 inch bore is a 1.75 inch rod, with $A_A/(2A_B) = 0.98$. The effect on hydraulic efficiency can be quantified using the steady-state model. Figure 20 shows plots of the hydraulic efficiency for a mid-range force of 50 kN, for a number of area ratios. This effect is small for commercially available cylinder sizes (on the order of 2% error), and only once other sources of loss are eliminated would one consider custom cylinders with the rod sized to sub-millimetre precision.

Conclusions

This paper presents a steady-state model of a dual-cylinder hydrostatic actuator (DCHA). A small-scale system was constructed to validate the models, which appear to be reasonably accurate. An analysis of a large-scale system for a backhoe loader was performed and the hydraulic efficiency is considerably higher than a conventional load-sensing system for the majority of operating points. Relative to a conventional valve-controlled system, the DCHA has the same maximum force, higher maximum velocity and can be constructed from commercially available components. In terms of cost and complexity, the DCHA is expected to be comparable to an electro-hydraulic load-sensing system, replacing the main control valve and load-sensing pump with on–off solenoid valves and a closed-circuit pump (with the substitution of two smaller cylinders if the application does not use

dual cylinders originally). Any additional cost can be expected to be quickly recovered via reduced fuel usage.

Disclosure statement

No potential conflict of interest was reported by the author.

Notes on contributor

Travis Wiens, PhD, PEng, is an assistant professor in the Department of Mechanical Engineering at the University of Saskatchewan. Prior to rejoining academia, he served as a consultant to the fluid power industry, particularly in the design of construction, forestry and mining equipment. His current research interests revolve around efficiency of hydraulic equipment, including pump-controlled architectures and digital hydraulics.

References

Achten, P. and Palmberg, J., 1999, What a difference a hole makes – the commercial value of the Innas hydraulic transformer. *Proceedings of the sixth scandinavian international conference on fluid power*, Tampere, 873–886.

Çalışkan, H., Balkan, T., and Platin, B.E., 2015. A complete analysis and a novel solution for instability in pump controlled asymmetric actuators. *Journal of Dynamic Systems, Measurement, and Control*, 137 (9), 091008.

Costa, G.K. and Sepehri, N., 2015. *Hydrostatic transmissions and actuators: operation, modelling and applications*. Chichester, UK: Wiley.

Ellman, A. and Piché, R., 1999. A two regime orifice flow formula for numerical simulation. *Journal of dynamic systems, measurement, and control*, 121 (4), 721–724.

Fales, R. and Raab, F., 2005, *Hydraulic control system with energy recovery*. US Patent US6854268 B2.

Grabbel, J. and Ivantysynova, M., 2005. An investigation of swash plate control concepts for displacement controlled actuators. *International Journal of Fluid Power*, 6 (2), 19–36.

Habibi, S., and Goldenberg, A., 1999, Design of a new high performance electrohydraulic actuator. *Proceedings of the IEEE/ASME international conference on advanced intelligent mechatronics*, IEEE, 227–232.

Hindman, J., 2006. *Hydraulic cylinder with Integrated Accumulator*. US Patent 7,104,052.

Jalayeri, E., *et al.*, 2015. A throttle-less single-rod hydraulic cylinder positioning system: design and experimental evaluation. *Advances in Mechanical Engineering*, 7 (5), 1–14.

Jarboe, H. Richard, 1983. *"Agricultural load-sensing hydraulic systems" ASAE Distinguished Lecture No 9*. Winter Meeting of American Society of Agricultural Engineering, Chicago, USA.

Lei, X., *et al.*, 2011. Study on simulation of digital pump-control cylinder position control system. *Procedia Engineering*, 16, 729–736.

Lux, J. and Murrenhoff, H., 2016. Experimental loss analysis of displacement controlled pumps. *In*: *10th international fluid power conference, dresden group I*, March, 441–452.

McCullough, K.R., 2011. *Design and characterization of a dual electro-hydrostatic actuator*. Hamilton: Department of Mechanical Engineering McMaster University.

Merritt, H.E., 1967. *Hydraulic control systems*. New York: Wiley.

Rahmfield, R. and Ivantysynova, M., 2001. Displacement controlled linear actuator with differential cylinder – a way to save primary energy in mobile machines. *Proceedings of the fifth international conference on fluid power transmission and control*, Hangzhou, 296–301.

van der Burgt, J.A.H., 1994. *A new approach to saving energy in cyclic loaded hydraulic systems: learning hydraulic systems*. Eindhoven University of Technology, Eindhoven, Netherlands.

Vukovic, M., Leifeld, R. and Murrenhoff, H., 2017. Reducing fuel consumption in hydraulic excavators—a comprehensive analysis. *Energies*, 10 (5), 1–25.

Wang, L., Book, W.J., and Huggins, J.D., 2011. A hydraulic circuit for single rod cylinders. *Journal of Dynamic Systems, Measurement, and Control*, 134 (1), 011019.

Weng, C.K., 1966. Transmission of fluid power by pulsating-flow (P-F) concept in hydraulic systems. *Transactions of the ASME Journal of Basic Engineering*, 88 (2), 316–321.

Wiens, T. and Bitner, D., 2016 An efficient, high performance and low-cost energy recovering hydrostatic linear actuator concept. *Proceedings of the ASME/BATH 2016 symposium on fluid power & motion control*, Bath, UK.

Williamson, C., and Ivantysynova, M., 2008. Pump mode prediction for fourquadrant velocity control of valveless hydraulic actuators. *In: Proceedings of the 7th JFPS international symposium on fluid power*, Toyama, Japan, 323–328.

Williamson, C. and Ivantysynova, M., 2010. Stability and motion control of inertial loads with displacement controlled hydraulic actuators. *In Proceedings of the 6th FPNI PhD Symposium*, June, West Lafayette, USA, 499–514.

Williamson, C., Zimmerman, J., and Ivantysynova, M., 2008. Efficiency study of an excavator hydraulic system based on displacement-controlled actuators. *Bath/ASME symposium on fluid power and motion control*, Bath, UK.